Domain structure and impurity length-scale effects in switching charge-density-wave conductors

M. F. Hundley and A. Zettl
Department of Physics, University of California, Berkeley, California 94720
(Received 9 October 1987)

We explore the internal structure and the relative coherence of sliding charge-density-wave (CDW) domains in switching crystals of pure and iron-doped $NbSe_3$. CDW domain coherence is examined by studying the current-voltage (I-V) characteristics when a temperature gradient is applied across a switching sample. We use a noninvasive voltage-probe technique to further determine the structure of switching domains. We find that drastically different results are obtained depending on the unperturbed nature of a sample's I-V characteristic, and suggest that this large variation in switching crystal I-V characteristics originates from differences in the distribution of the switch-causing ultrastrong impurities. These results are discussed in terms of a phase-slip model of switching.

I. INTRODUCTION

The intriguing nonlinear electrical conductivity observed both in $NbSe_3$ and other quasi-one-dimensional materials has been extensively studied during the past decade.[1] The nonlinear conductivity stems from the depinning and subsequent Fröhlich motion of the charge-density-wave (CDW) condensate. This sliding motion occurs when an applied electric field E exceeds the CDW pinning threshold field E_T. CDW depinning is usually evident in the current-voltage (I-V) relationship as a smooth, continuous change from the pinned, linear state to the higher conductance sliding, nonlinear state. At fields well past E_T the CDW conductance saturates and the differential resistance becomes field independent.

Not all CDW samples display a smooth depinning process in their I-V characteristics. In some CDW crystals, the CDW depins in a sharp, hysteretic manner which gives rise to a strong discontinuity in the I-V curve. This phenomenon was first observed in the low-temperature state of $NbSe_3$ and is referred to as *switching*.[2] The dynamic switching state is characterized by a temperature-independent depinning field,[3] hysteresis,[4] negative differential resistance,[5] period-doubling routes to chaos,[6] and inductive ac response.[7] Switching has also been observed in many other CDW materials which show nonlinear transport, including TaS_3,[8] $K_{0.3}MoO_3$,[9] and $(NbSe_4)_{3.33}I$.[10] Switching can also be enhanced or induced by iron-doping $NbSe_3$ (Ref. 11) or by irradiating either TaS_3 or $K_{0.3}MoO_3$.[12] This suggests that switching is caused by the interaction of impurities with the CDW.

Switching in both $NbSe_3$ and Fe_xNbSe_3 is associated with the separation of the CDW into distinct, serially arranged macroscopic phase-velocity coherent domains.[13] The domains are separated by localized phase-slip centers which are presumed to consist of ultrastrong impurity sites.[14] According to a phase-slip switching model,[14–16] switching occurs when the CDW amplitude at an ultrastrong pinning site collapses due to the strong phase polarization which builds up there in the presence of a dc bias field. This phase and amplitude dynamical model has been successful in accounting for the physical behavior displayed by switching CDW crystals.[15,16]

While all switching samples show abrupt and discontinuous CDW depinning, there is a wide diversity in the I-V character of switching samples of $NbSe_3$. However, the I-V characteristics of switching crystals can be loosely classified into two categories and this classification will become important in discussing the experiments described in this paper. In what we call type-I samples, the CDW depins largely via a single predominant switch, although other, much smaller switches might also be present in the I-V curve. These large type-I switches generally show a large amount of hysteresis which is accompanied by the formation of switching sublevels within the hysteresis loop.[4] Type-II samples depin via a number of much smaller, roughly equal-sized switches and display only small amounts of hysteresis. No sublevels are evident in the I-V characteristics of type-II samples. While the physical ideas which are embodied in a phase-slip switching model[14–16] successfully describe the underlying mechanisms which cause switching, it is far from obvious if the model can account for the large diversity observed in the I-V characteristics of switching CDW crystals.

In this paper we present the results of a study of switching in both $NbSe_3$ and Fe_xNbSe_3 that was performed in order to clarify the differences between type-I and type-II switching behavior. To determine the underlying differences between these two classes of switching behavior we have employed two techniques that probe the distribution, structure, and relative coherence of switching domains. In the first technique, thermal gradients are applied across the length of switching samples. The resulting effects upon the switches in an I-V curve indirectly indicate the coherence and internal structure of switching domains. In the second technique, the locations of these domains are mapped out by using a noninvasive domain localization voltage probe. By using these techniques we determine that the drastically different switching behavior observed in different crystals of these materials is a direct result of differences in the distribution of the ultrastrong impurities contained within them. This behavior is found to be consistent within the framework of a phase-slip model of switching.[15,16]

The remainder of this paper is organized in the follow-

ing manner. Section II describes the materials and methods used in this study. Our experimental results, presented in Sec. III, are followed by an analysis in Sec. IV. Finally, we briefly summarize our findings and present concluding remarks in Sec. V. Some of the experimental results presented here have been previously presented.[17]

II. MATERIALS AND EXPERIMENTAL TECHNIQUES

Samples used in this research consisted of single crystals of high-purity $NbSe_3$ and Fe_xNbSe_3 that were produced by the conventional vapor-transport method. The amount of iron which was incorporated into the Fe_xNbSe_3 was much smaller than the nominal doping level ($x \approx 0.03$); it was below the 1% sensitivity of microprobe analysis.[14] Typical crystal cross-sectional dimensions for both $NbSe_3$ and Fe_xNbSe_3 were 5×3 μm^2. Crystal lengths varied from 0.3 to 1.5 mm.

The experimental configuration consisted of single switching crystals suspended in vacuum between either two large copper mounting posts anchored to Peltier heater chips or between a pair of sapphire blocks with Manganin heater wire wound about their bases. Electrical contacts were made at the ends of the crystal with silver conductive paint. Thermometry was accomplished by a diode sensor and several miniature differential thermocouples. All I-V curves presented in this paper were measured using a current-driven configuration.

The domain localization technique was employed to more directly map out the switching domains in these materials. In this technique current domains are observed by nonperturbative measurements of local dc conductivities.[13,14] The method uses a three-terminal probe. A pair of current leads, terminals 1 and 3, are attached to either end of a crystal using silver conductive paint. The third probe, terminal 2, is a nonperturbing voltage-sensing lead composed of fine 2.54-μm-thick Wollaston (Rh-Pt) wire which can be lightly pressed against the sample. The location of this probe could be varied along the entire length of the sample with its absolute position determinable to within an accuracy of ± 5 μm. By measuring the I-V characteristics of various sections of a given switching sample, the number and location of the switching domains can be directly determined. Fine Wollaston wire was used so as to minimize any mechanical and current distribution perturbations and, when in the presence of a temperature gradient, thermal perturbations at the point where the probing wire touches the sample.

III. EXPERIMENTAL RESULTS

In the subsections that follow we describe the application of both the thermal gradient and the domain localization techniques to switching samples of $NbSe_3$ and Fe_xNbSe_3. The results from experiments on type-I $NbSe_3$ are presented first. This is followed by the results from experiments on type-II $NbSe_3$ and Fe_xNbSe_3.

A. Type-I $NbSe_3$

The zero-gradient I-V characteristics of a typical type-I switching sample of $NbSe_3$ at temperatures between 24.6 and 29.3 K are presented in Fig. 1. The data clearly show that the switch depinning threshold current, I_T, is a decreasing function of temperature in the switching regime. This particular crystal shows negative differential resistance at 29 K and clear switching below 27 K. Below 26 K the CDW depinning proceeds via two independent switches, labeled S_1 and S_2 in the figure. The first switch, S_1, is much larger than switch S_2. This suggests that in isothermal conditions the crystal consists of two macroscopic current-carrying domains. These two domains are probably separated by a phase-slip center. The two switches become hysteretic below 25.5 K, and no additional switches are observed at temperatures less than 24 K.

The effects of a temperature gradient on two type-I switching crystals with widely different lengths are shown in Fig. 2. The data in Fig. 2(a) show the effects of a temperature gradient on the I-V characteristics of the same 300-μm-long sample examined in Fig. 1, while Fig. 2(b) shows the thermal gradient I-V characteristics of a different type-I switching sample which is 1.5 mm in length. We first consider the results presented in Fig. 2(a). In this case, the temperature of one end of the sample was held fixed at $T_0 = 24$ K while the other end was warmed to a higher temperature, $T_0 + \Delta T$, ranging between 24 and 28 K. The curves in Fig. 2(a) are labeled by the temperature difference ΔT. The data in Fig. 2(a) demonstrate that applied thermal gradients have a strong effect upon the switching characteristics of type-I $NbSe_3$. As the temperature gradient is increased, the dominant

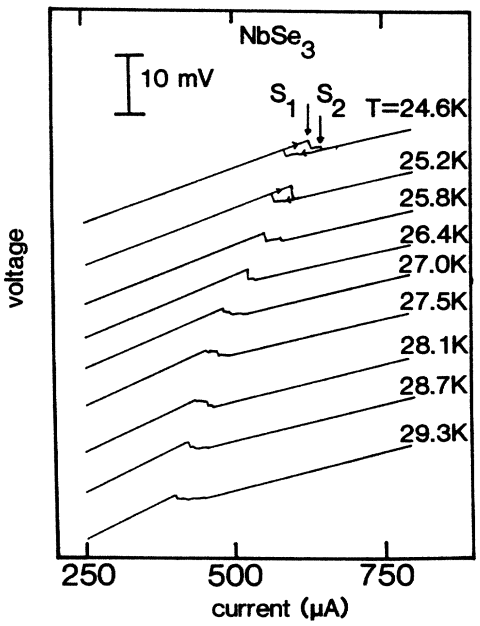

FIG. 1. Zero-gradient current-driven I-V characteristics for a type-I $NbSe_3$ switching crystal at temperatures between 24 and 29 K. At low temperatures two distinct hysteretic switches, S_1 and S_2, occur and are identified by the vertical arrows.

switch, S_1, appears to break up into a series of smaller switches. These subswitches are labeled S_1', S_1'', S_1''', and S_1'''' in the $\Delta T = 2.3$ K trace in Fig. 2(a). As the gradient is increased in strength the lowest threshold switch S_1' seems to depin at progressively lower threshold currents. In the process of moving to lower threshold currents, switch S_1' appears to break apart, shedding the smaller switches S_1'', S_1''', etc., and in so doing becomes smaller in size. The smaller switches continue to move to lower threshold currents as the gradient is increased. The smaller switch S_2 appears essentially unaffected by the temperature gradient.

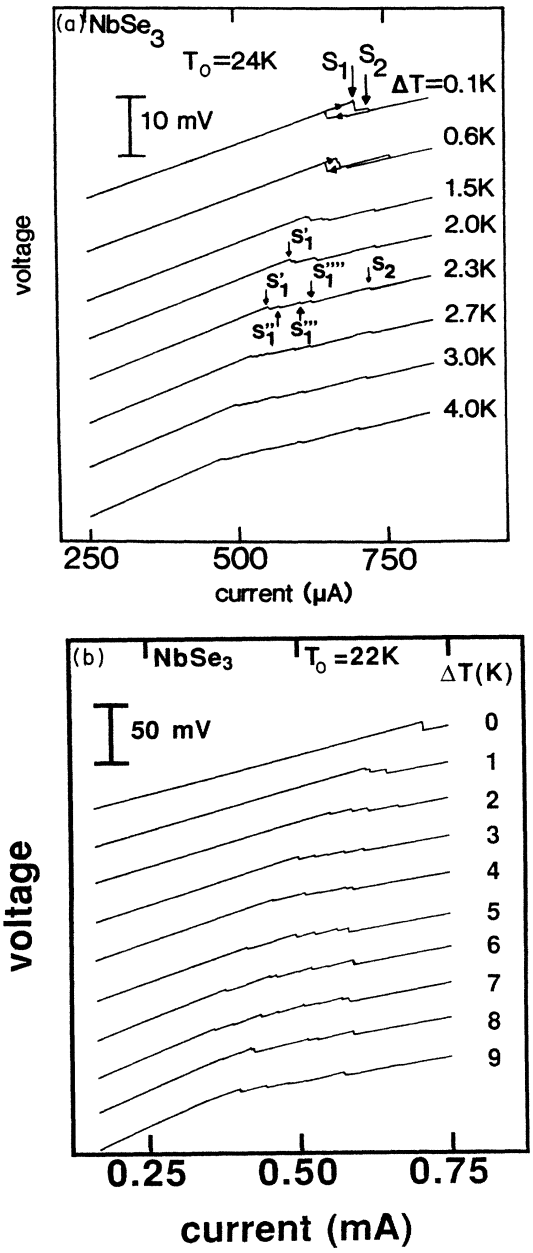

FIG. 2. (a) Current-driven I-V characteristics for the same type-I $NbSe_3$ sample used in Fig. 1, but in the presence of a temperature gradient. The cold end of the sample is held at $T_0 = 24$ K while the hot end is at $T_0 + \Delta T$. With increasing ΔT, switch S_1 breaks up into a series of smaller switches S_1', S_1'', etc., as identified in the $\Delta T = 2.3$ K trace. (b) Thermal gradient I-V characteristics of a type-I switching sample that is five times as long as that used in (a).

The thermal gradient effects on the I-V characteristics of the crystal of length $L_s = 1.5$ mm are shown in Fig. 2(b). In this case the temperature of one end of the sample was held fixed at $T_0 = 22$ K while the other end was heated to a temperature of $T = T_0 + \Delta T$, ranging between 22 and 31 K. With $\Delta T = 0$ this sample depins via a single extremely large switch with a magnitude of $\Delta V = 10$ mV, some three times larger than that of switch S_1 in Fig. 2(a). The thermal gradient acts to break the isothermal switch into a series of small subswitches which continue to spread apart in the I-V curve as the gradient is increased. As in Fig. 2(a), the number of switches rises as the gradient increases in magnitude, reaching a maximum value of roughly eight at $\Delta T = 7$ K. Above $\Delta T = 8$ K the minimum-threshold switch begins to depin in a nonswitching fashion, indicating that the hot end of the sample is outside of the switching temperature regime (for this sample $T_{\text{switch}} \lesssim 30$ K). The general behavior observed in both of these samples is not unique: the thermal gradient switch break-up has been observed in all type-I switching samples which we have examined.

We associate the temperature gradient behavior of Figs. 2(a) and 2(b) with the underlying domain structure of these type-I samples. The I-V characteristics in the presence of a thermal gradient clearly show that the zero-gradient domains which give rise to switch S_1 in Fig. 2(a) and the extremely large switch in Fig. 2(b) are actually composed of a number of subdomains. These numerous subdomains can only be seen in the I-V curve when stress, here in the form of a temperature gradient, is applied to the sample. For the 0.3-mm-long sample used for Fig. 2(a) this is demonstrated more clearly in Fig. 3(a), where the depinning threshold current of switch S_1' is plotted as a function of temperature [assuming $T(\text{domain } S_1') = T_0 + \Delta T$], along with the temperature dependence of the threshold current of the zero-gradient switch S_1 as deduced from Fig. 1. Similar data for the 1.5-mm-long sample of Fig. 2(b) are shown in Fig. 3(b). In both cases the two thresholds match closely throughout the respective temperature ranges. These data indicate that the domains which give rise to the large switches in the isothermal I-V curves in Figs. 2(a) and 2(b) are actually composed of a number of subdomains. In the absence of a thermal gradient these subdomains appear to depin in unison, creating a large zero-gradient switch. As a thermal gradient is applied and increased in strength, the subdomains decouple and depin according to their own local temperature. Since $I_T \sim 1/T$ (see Sec. IV), the hotter subdomains must depin at progressively lower currents as the gradient is increased.

By examining the way in which the large zero-gradient switches decompose as the temperature gradient is increased in strength, it appears that these subdomains must actually be strongly coupled together, making them depin in a synchronized fashion when $\Delta T = 0$. This becomes evident when we consider three important aspects of the small thermal gradient data in Figs. 2(a) and 2(b).

First, the number of subswitches increases as the gradient is increased; this indicates that the neighboring subdomains are linked together since, with no such linkage, the subdomains would all depin at different threshold currents even in the presence of small gradients (this would cause the zero-gradient switch to become smoothly "smeared" in the limit of low thermal gradients). Second, the subswitches appear to break off from the larger switch one at a time as the larger switch decomposes in a thermal gradient. This larger switch continues to move to lower thresholds as it sheds the subswitches. As the gradient increases the "main" switch becomes as small as the decoupled subswitches and stops devolving further. This suggests that the coupled subdomains depin together in the absence of a thermal gradient; the depinning of this large "train" of switching subdomains creates a large type-I switch. As a gradient is applied, single subdomains break off from the main group, giving rise to the isolated switches in the I-V curve. As the gradient is increased further, more and more subdomains decouple until all of them are depinning independently. The third piece of evidence which suggests that the grouped subdomains depin in a synchronized fashion is that the data in Figs. 3(a) and 3(b) match the zero-gradient thresholds even in small gradients sufficient to split the sample into only two domains. Hence, the train of coupled subdomains near the hot end of the sample do not act as if they were depinning at their average temperature (somewhere between T_0 and $T_0+\Delta T$), but rather at the hot-end temperature of $T_0+\Delta T$. This indicates that the subdomain at the hot end, with $T=T_0+\Delta T$, must be depinning first, and in turn triggering all the other subdomains which are coupled to it. This seems plausible in light of the fact that the "hot" subdomain may have a smaller threshold current than all the other subdomains since $I_T \sim 1/T$. Thus, the temperature gradient I-V curves in Figs. 2(a) and 2(b) suggest that large type-I switching domains actually consist of a number of subdomains which depin in a synchronized manner as long as no thermal gradients are present across the length of the crystal.

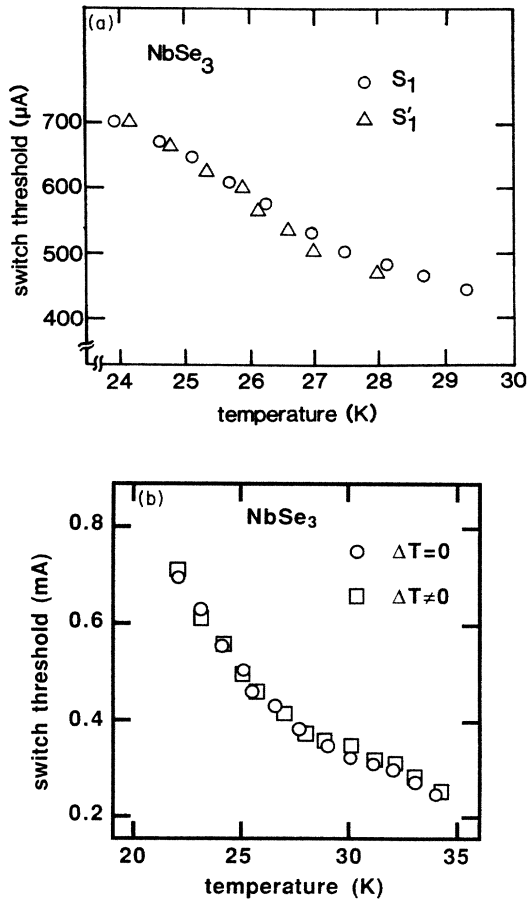

FIG. 3. (a) Threshold current vs temperature for switching to occur in the same type-I $NbSe_3$ crystal used in Figs. 1 and 2(a). The open circles refer to switch S_1 of Fig. 1 (zero gradient) while the triangles refer to the first switch S_1' of Fig. 2(a) (with a gradient). The temperature used when plotting $I_T(S_1')$ is $T_0+\Delta T$. The close correspondence of the two data sets indicates that S_1' is associated with a switching current domain very near the "hot" end of the sample. (b) Switching threshold current vs temperature corresponding to the data presented in Fig. 2(b). The open circles refer to the threshold in the absence of a thermal gradient. The squares show the minimum switching threshold in the presence of a temperature gradient, assuming $T=T_0+\Delta T$.

In order to verify the existence of these subdomains, we attempted to perform domain localization experiments on type-I switching samples. This technique has been successfully used to map out the domain structure in switching Fe_xNbSe_3 crystals.[13] Unfortunately it is impossible to apply the "nonperturbing" voltage probe to type-I switching samples without drastically altering the I-V characteristics. The character of the depinning switch is measurably changed regardless of how finely the probing wire is laid across the sample. Generally, a type-I sample, which normally depins via a single large switch in the absence of the movable voltage probe, will depin via a number of much smaller switches due to the physical perturbation applied by the mechanically touching probe wire. This effect is shown in Fig. 4, where a type-I sample which depins by way of a single switch displays two switches under the influence of the voltage probe. No temperature gradient is applied in either case. Hence, switching samples which are perturbed by a thermal gradient are also extremely sensitive to the slight mechanical stress brought on by the external probe.

The thermal gradient and probe pressure effects on type-I switching samples indicate that they are composed of many small switching domains. In the absence of external perturbations, these subdomains depin in a synchronized fashion, manifesting themselves in an I-V trace as a single, large switch. Only by perturbing the system can the coupling between subdomains be reduced sufficiently to show this underlying subdomain structure. Attempts at domain localization show that the interdomain coupling is also very sensitive to external mechanical perturbations. The existence of many subdomains in type-I samples suggests that switch-causing ultrastrong impurities are closely spaced within type-I samples.

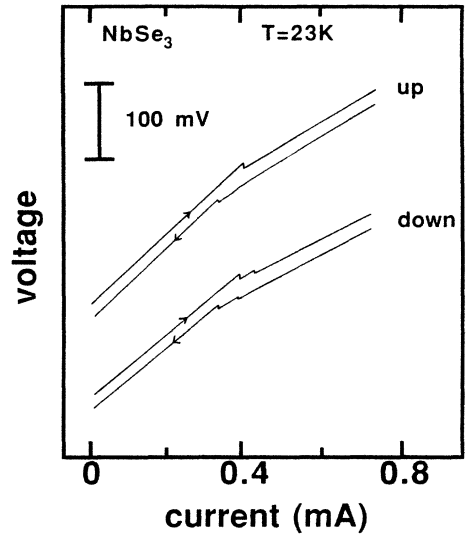

FIG. 4. Change in I-V characteristics of a type-I switching sample when a fine movable voltage probe is touching ("down") and not touching ("up") the crystal. The perturbing 0.1-mil Wollaston wire was placed in the middle of the sample, halfway between both end contacts. All traces have been vertically offset for clarity.

B. Type-II $NbSe_3$

The effects of an applied temperature gradient on a type-II $NbSe_3$ switching sample of length $L_s = 1.40$ mm are shown in Fig. 5. The zero-gradient trace indicates that this sample depins by way of four separate switches in an isothermal configuration. As displayed in Fig. 5, thermal gradients do not break down these switches into a larger number of small switches. The thermal gradient

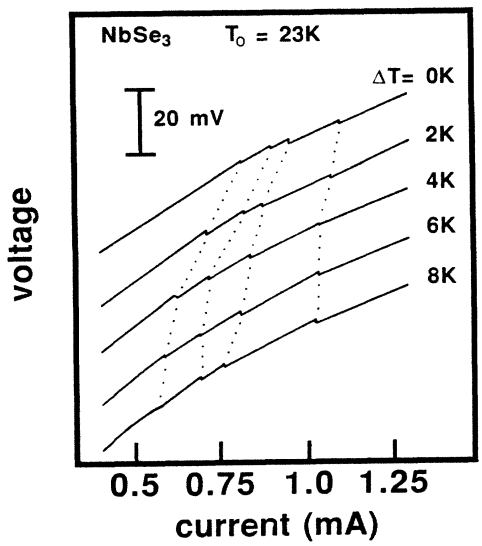

FIG. 5. Current driven I-V characteristics in a temperature gradient for a type-II $NbSe_3$ crystal. In this sample the original four switches do not divide into smaller switches when the gradient is applied. The dotted lines are guides to the eye showing the progression of switching onsets as the gradient is varied.

only acts to move the switching onsets to lower threshold currents, as expected when each local switching domain is raised in temperature. Note that the applied gradient was sufficient to heat the first depinning domain out of the switching regime.

These data indicate that type-II switching domains cannot be decoupled into subdomains even in gradients sufficient to cause decoupling in type-I samples. As an example, the data in Fig. 2(b) indicate that this type-I sample is divided into roughly ten domains by a 5-K/mm gradient, while the data shown in Fig. 5 indicate that this type-II sample consists of only four subdomains even in thermal gradients as large as 10 K/mm. Similar results have been obtained when studying other type-I and type-II samples. Hence, it would appear that type-II zero-gradient switching domains are not composed of further subdomains, in contrast to the type-I samples discussed previously.

We have performed domain localization measurements on these type-II samples. The localization results for the same sample that was used for Fig. 5 are presented in Fig. 6. Unlike type-I samples, type-II switching crystals are essentially unaffected by the mechanical stress that results from the placement of the movable voltage probe. The I-V measurements obtained with the movable contact positioned in the middle of the sample [as indicated in Fig. 6(a)] are depicted in Fig. 6(b). The position of the many switching domains contained within this sample can be roughly determined by examining the I-V characteristics on either side of the adjustable contact. In order to more precisely determine the location and arrangement of these domains, eight sets of I-V curves were measured with the middle contact position ranging between contacts 1 and 3. The domain arrangement determined experimentally is depicted in Fig. 6(c). These results show a very strong current polarity dependence on the switching characteristics. With the current flowing in one direction the CDW depins by way of five switches, while when flowing in the opposite direction the CDW depins via only three switches. Note that the location of the interfaces between switching domains are also different for the two current polarities. Hence, different ultrastrong pinning sites are activated and cause switching to occur when the current flow direction is reversed. The diagram in Fig. 6(c) also indicates that the switching domains need not be serially arranged. In general, switching domains occur side-by-side transversely only if they are located adjacent to a current contact. This suggests that nonserially arranged switching domains may be a result of irregular current injection near a current contact. The domain arrangement of Fig. 6(c) remained unchanged when a thermal gradient was applied across the sample.

The absence of temperature gradient decoupling effects in type-II samples suggests that there are no subdomains in these crystals and that neighboring domains do not couple together when depinning. This is also borne out by the fact that the movable voltage probe acts in a nonperturbing manner when positioned on a crystal. Thus, type-II crystals consist of a relatively small number of large switching domains which are internally homogene-

ous. These large domains presumably do not couple together in a synchronized depinning process due to the presence of a chemical gradient within the samples. Because the crystal is already separated into multiple domains, an applied thermal gradient is unable to break the sample into more subdomains. The chemical gradient which causes this behavior may be in the form of large variations in either the local impurity or lattice defect concentrations. In either case the data suggest that type-II samples contain fewer, more widely spaced ultrastrong impurities than do type-I samples.

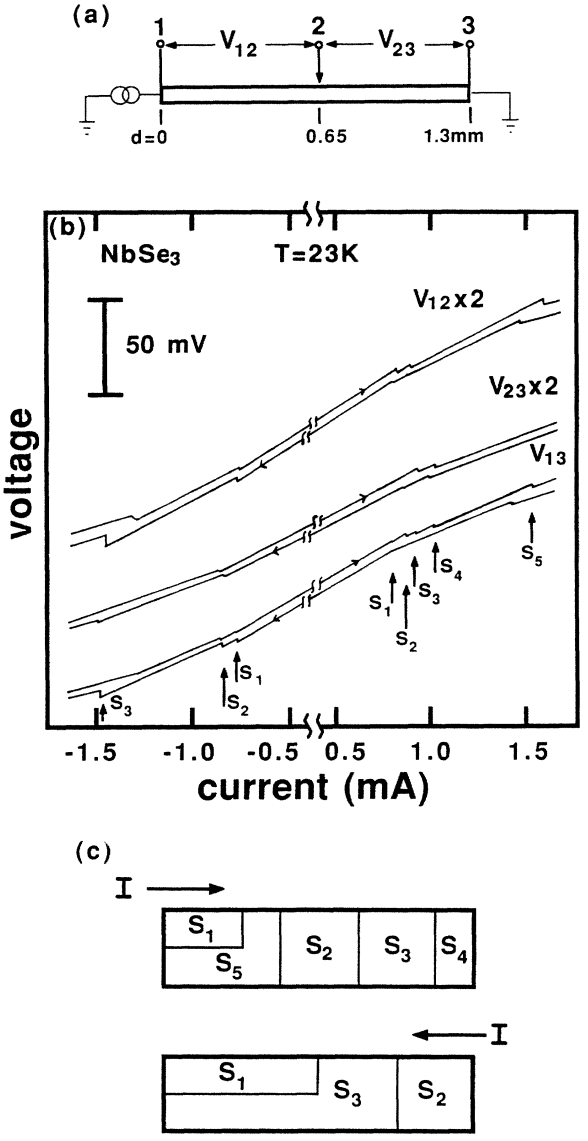

FIG. 6. (a) Voltage-probe configuration for I-V traces shown in (b). (b) Simultaneously recorded current-driven I-V traces for different segments of a type-II $NbSe_3$ switching crystal at $T=23$ K. The traces for increasing and decreasing bias sweeps have been vertically offset for clarity. (c) The arrangement of the switching domains in the sample studied in (b) as determined by the domain localization technique. The current direction is indicated in both diagrams. The switches are labeled S_i, where the index indicates the depinning order.

C. Fe_xNbSe_3

Switching in iron-doped $NbSe_3$ differs subtly from that observed in the pure material. In addition to occurring at higher temperatures, the size of the switching voltage discontinuity ΔV in Fe_xNbSe_3 is usually not as large as in pure $NbSe_3$.[14] In type-I $NbSe_3$ the switching voltage discontinuity can be as large as $\Delta V \approx 10$ mV while it is generally no more than 1 mV in Fe_xNbSe_3. Iron-doped switching samples depin via single or multiple switches, show only small amounts of hysteresis, and never display any hysteretic switching sublevels. Thus, switching in Fe_xNbSe_3 belongs to the type-II classification.

The results from both temperature gradient and domain localization experiments on $NbSe_3$ clearly show that these techniques can be used to infer the distribution of switching impurities within a crystal. For this reason we have applied these techniques to switching samples of Fe_xNbSe_3. In light of the fact that the incorporation of iron tends to cause switching in $NbSe_3$, these techniques should provide a means of indirectly determining the distribution of iron in this material. In particular, this study was carried out to determine if the iron is incorporated in a uniformly distributed manner or if it tends to cluster in a highly localized fashion.

The thermal gradient effects on a sample of Fe_xNbSe_3 which depins by way of a single switch is shown in Fig. 7. The thermal gradient only moves the switching onset to lower threshold currents and does not cause the switch to break down into a series of smaller switches. The same results have been obtained on other samples of Fe_xNbSe_3 which depin via more than one switch. These results suggest that iron-doped samples consist of widely spaced impurities and large switching domains.

To more directly determine the domain structure of this sample we performed a domain localization experiment similar to the one described above for type-II $NbSe_3$. A typical set of I-V traces are shown in Fig. 8(b),

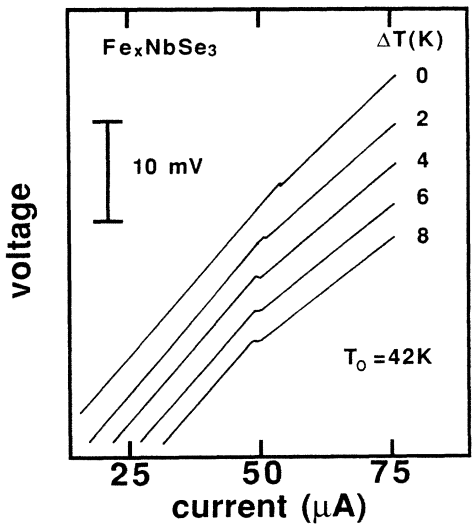

FIG. 7. Thermal gradient effects on Fe_xNbSe_3. The cold end of the sample was held fixed at $T_0=42$ K while the hot end was heated to $T_0+\Delta T$.

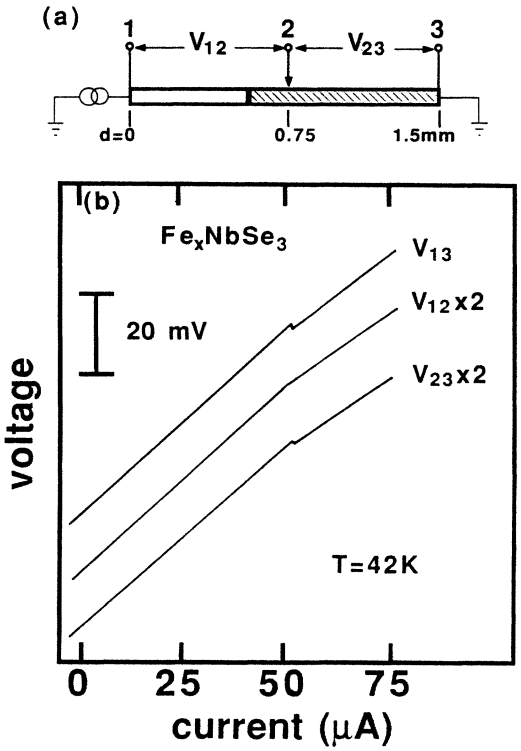

FIG. 8. (a) Voltage-probe configuration for *I-V* traces shown in (b). (b) Simultaneously recorded current-driven *I-V* traces for different segments of a Fe_xNbSe_3 crystal at $T_0=42$ K. In this instance the nonperturbing contact was located near the interface between the two CDW domains.

with the movable probe positioned as indicated in Fig. 8(a). Localization traces indicate that $\frac{5}{8}$ of the sample consists of a switching domain [the hatched region in Fig. 8(a)]. The remainder of the sample does not cause a discontinuity in the sample voltage when it depins (both of these domains depin at roughly the same threshold current). These results are similar to those of previous studies of Fe_xNbSe_3.[13] In all cases, Fe_xNbSe_3 is far less affected by the movable voltage probe than are samples of type-I $NbSe_3$.

These results show that iron-doped switching samples contain large switching domains, indicating that the switch-causing impurities in Fe_xNbSe_3 are widely separated. This suggests that the iron is not uniformly incorporated into the doped $NbSe_3$. Switching in Fe_xNbSe_3 is characterized by large switching domains, no domain coupling, and no external perturbation effects.

IV. ANALYSIS

Even in *non*switching CDW samples, it has been observed that applied temperature gradients cause the CDW condensate to break up into separate and distinct current-carrying domains.[18–22] This is because of the strong temperature dependence of the parameters which characterize the CDW condensate. The experiments described above also exploit the temperature dependence (and temperature independence) of CDW parameters in switching crystals.

In a simple approximation, the electronic charge density in a CDW may be represented by

$$\rho(x)=\rho_a+\rho_c\cos[2k_Fx+\phi(x)]\ , \tag{1}$$

where ρ_a is the average electronic density, ρ_c is the amplitude of the density wave, k_F is the Fermi wave vector, and $\phi(x)$ is the position-dependent phase of the CDW; motion or distortion of the wave is accounted for by the phase variable $\phi(x)$. In the presence of a bias current I which exceeds the depinning threshold current I_T the CDW will slide with a velocity $v(x)$ related to the time derivative of the phase. This phase velocity depends on the parameters which characterize the CDW,

$$v(x)\propto\frac{d\phi(x)}{dt}=f(\rho_0(T(x)),n_c(T(x)),E_T,I)\ , \tag{2}$$

where ρ_0 is the low-field resistivity, n_c is the CDW electron density, and E_T is the CDW threshold electric field. In Eq. (2) we explicitly indicate that both ρ_0 and n_c are functions of temperature while E_T is *independent* of temperature in a switching crystal.[3] The CDW phase velocity is independent of the position coordinate x within a CDW domain because of the form of the phase distortion term in the CDW Hamiltonian[23]

$$H_{\text{elastic}}=\tfrac{1}{2}\kappa\int|\nabla\phi|^2d^3x\ , \tag{3}$$

where κ is the CDW phase elasticity coefficient. If $d\phi/dt$ were a function of position, the phase gradient $\nabla\phi$ would steadily increase with time and result in the destruction of the CDW. Hence, a stable sliding CDW must form phase-velocity coherent domains.

When a temperature gradient is applied across the length of a sample [$T(x)=T_0+(\nabla T)x$, $0<x<L$] Eq. (2) would suggest that the local phase velocity must become a function of position. This is at odds with the requirement that the CDW phase velocity be constant in order to keep the phase distortions from destroying the sliding CDW. To ensure that the sliding CDW is stable in a thermal gradient, subtle local phase distortions must occur which cause the entire domain to move at a velocity v_0. These distortions will act to slow down CDW regions where otherwise $v(x)>v_0$ and speed up CDW regions where otherwise $v(x)<v_0$. Hence, the phase velocity of a domain becomes constant at the expense of creating phase distortions along the length of the domain. These phase distortions raise the energy of the CDW as indicated by Eq. (3). The degree to which the CDW energy increases will depend upon how much the domain velocity v_0 and $v(x)$ differ. This velocity mismatch will depend on the applied temperature difference ΔT as well as the sample length L. As a result, there can exist the situation where the energy increase due to the presence of the thermal gradient can be minimized if the domain were to split into a number of subdomains. With many smaller subdomains the domain velocity "mismatches" and the resulting phase distortions can be reduced. Hence, under certain conditions it can be energetically favorable for a CDW domain in the presence of a temperature gradient to break into a number of subdomains. Each domain will move at a different velocity corresponding to its local

average temperature. In this situation, the interface between neighboring subdomains must act as a phase-slip center because of the discontinuity in the CDW domain velocities. The CDW amplitude must periodically collapse at these phase-slip centers in order to link neighboring subdomains together.

It is energetically very costly to create a phase-slip center unless large impurities exist within a domain. Hence, uniform and coherent switching domains will not, in general, be broken down into subdomains by a thermal gradient (this is the behavior of type-II samples). In the opposite case of domains which are nonuniform and contain many large impurity centers the CDW will, under the action of a temperature gradient, readily split into subdomains so as to lower the overall energy of the system (this is the behavior of type-I samples).

In the case of type-I samples, once the subdomains are decoupled from the neighboring sections of the CDW they will behave according to their own local average temperature. This decoupling process can be observed by measuring the current-driven I-V characteristics of a crystal. The switching threshold current I_T will be

$$I_T(T)=\frac{aE_T}{\rho_0(T)} , \tag{4}$$

where a is the sample cross-sectional area and we explicitly indicate that ρ_0 is a function of temperature while E_T is not. In the temperature region studied here, ρ_0 is an increasing function of temperature ($\rho_0 \sim T$) in both $NbSe_3$ and Fe_xNbSe_3, and the threshold current will therefore drop with increasing temperature ($I_T \sim 1/T$). Hence, in the presence of a thermal gradient each decoupled subdomain will depin at a threshold current which is determined solely by its local temperature.

The thermal gradient effects on a sample's current-driven I-V characteristics therefore indicate whether or not the zero-gradient domains are internally uniform and coherent. If a domain is internally uniform (i.e., there are no ultrastrong impurities contained within it) the switch should be unaffected by the temperature gradient. On the other hand, if a domain contains a number of ultrastrong impurities, the switch caused by its zero-gradient depinning will decompose into a number of smaller subswitches in the presence of a thermal gradient. These subswitches will each depin according to their local temperatures and will therefore be separated into the resulting I-V curve. Hence, by observing the thermal gradient effects on a switching I-V curve one can indirectly determine the uniformity, internal structure, and relative coherence of a zero-gradient switching domain, as we discuss further below.

Our localization experiments on switching samples are in agreement with earlier work which indicated that the sliding CDW in switching samples breaks up into separate and distinct phase-velocity coherent domains.[13,14] Each switching domain depins at a unique threshold field and moves at a unique field-dependent velocity. This means that discontinuities in the CDW velocities must exist at the interface between adjacent switching domains. This requires that a phase-slip center must exist in the region between the neighboring domains in order to tie together the CDW phase across this interface. CDW amplitude dynamics must play an important role in this phase-slip process. We consider the Fukuyama-Lee-Rice CDW dynamic phase Hamiltonian[23]

$$H=\frac{\kappa}{2}\int d^3x \mid \nabla\phi \mid^2 + W_0\rho_a \sum_i \cos[2k_F x_i+\phi(x_i)] + \int \frac{e\rho}{2k_F}\phi E\, dx , \tag{5}$$

where κ is the CDW elastic constant, W_0 is the impurity potential, and ρ is the charge density. The three terms in Eq. (5) are related to the CDW phase elasticity, the CDW interaction with impurities at x_i, and the CDW interaction with an external electric field E, respectively. This expression intentionally neglects any fluctuations in the CDW amplitude, assuming instead that the amplitude is always constant. This Hamiltonian cannot describe the CDW in the vicinity of a phase-slip center because it is invalid in the limit of large phase polarization $\nabla\phi$. To see this, consider a moving CDW domain d_1 ($v_1>0$) adjacent to a nonmoving domain d_2 ($v_2=0$). The CDW phase will become highly polarized and distorted in the interface region between d_1 and d_2 as the CDW phase piles up there. This phase pileup and distortion will affect the system in two ways. First, the large phase polarization in the interface region will force the CDW amplitude to collapse there. This comes about because the phase polarization effectively changes the CDW wave vector. The CDW amplitude is determined by balancing the lattice energy cost of the Peierls distortion against the electronic energy gained from forming the CDW; the CDW amplitude must diminish when the CDW wave vector is distorted away from $Q=2k_F$. Hence, the CDW amplitude must collapse due to the strong buildup of phase distortion in the interface region between the two domains. When the amplitude is collapsed, the CDW phase can jump by a factor of 2π so as to reduce the phase distortion, thus completing a cycle of the phase-slip process.[16] The large phase polarization will also act as a pinning force on the moving CDW domain; only because of the periodic collapse of the CDW amplitude in the interface region can the domain continue to slide. Thus, the CDW velocity discontinuities in switching crystals suggest that amplitude dynamics as contained in the phase-slip process are very important in switch depinning.

To ensure that the phase-slip process is the primary cause of switching we must again consider a pair of neighboring domains d_1 and d_2, where in this case domain d_1 is only weakly pinned while the small domain d_2 is pinned so strongly that it cannot be depinned by an electric field. When an electric field is applied to this domain system the phase in d_1 will become polarized in the direction of d_2. Because the CDW in d_2 is pinned, domain d_1 will not depin in the usual fashion even when the bias field exceeds its weak pinning threshold field. As the bias is increased further the phase polarization in the interface between the two domains will increase until $\nabla\phi$

is so large that the CDW amplitude in the interface must collapse. At this point the polarization pinning forces holding d_1 back disappear and the domain can depin; it will switch to a high-field state because the bias necessary to cause the amplitude collapse is far higher than the weak pinning threshold field. At the same time, the phase in the interface region is free to change so as to relieve the phase polarization stress. The phase will slip by a factor of 2π to relieve the stress while still minimizing the impurity potential energy of domain d_2. After this phase-slip process the CDW amplitude will reform (because the phase difference has been reduced by 2π), and the CDW polarization will again increase, leading to another sequence of the phase-slip process.

The phase-slip switching mechanism requires there to be small regions where the CDW is strongly pinned to the lattice. This is corroborated by the fact that switching can be induced in $NbSe_3$ by iron doping, or in $K_{0.3}MoO_3$ by irradiation damage. These results suggest that the presence of impurities within a crystal play an important role in creating switch-causing phase-slip centers. The most energetically efficient phase-slip process consists of the formation of phase vortices.[24,25] In this type of phase-slip process the CDW velocity discontinuities are relieved by a stream of phase vortex cores which run perpendicular to the direction of CDW motion. The energy of a single phase vortex is[14]

$$E_{\text{phase-slip}} = N_0 \Delta^2 \xi^3 [1 + \alpha \ln(L_0/\xi)] , \tag{6}$$

where $\alpha = \kappa/(N_0\Delta^2\xi^2)$, N_0 is the density of states at the Fermi surface, Δ is the CDW energy gap, κ is the CDW elastic constant, L_0 is the CDW phase coherence length, and ξ is the amplitude coherence length. The first term in Eq. (6) corresponds to the energy of the vortex core while the second term relates to the phase distortion in the vicinity of the vortex. This phase-slip energy is far greater than the impurity pinning strength of conventional weak or strong impurities. Hence, the phase-slip centers in switching CDW crystals must be created by the presence of far stronger impurities which we call ultrastrong impurities.[13,14] These ultrastrong impurities could consist of extremely large strong-impurity concentrations; they might also be a result of dislocation lines or, in the case of Fe_xNbSe_3, phase inclusions. Regardless of their exact physical nature, ultrastrong impurities so strongly pin the CDW near them that they create phase-slip centers which in turn cause weakly pinned neighboring sections of CDW to undergo switch depinning.

The development of a complete model of CDW switching dynamics necessitates a system Hamiltonian which includes both CDW phase and amplitude dynamics. Such a Hamiltonian has not yet been established. Here we consider a simple dynamical model[15,16] of switching based on the physical mechanisms involved in the phase-slip process discussed above.[26] The model can be understood by considering a weakly pinned CDW domain d_1 adjacent to a small section of CDW d_2 which contains an ultrastrong impurity. In addition to the usual weak pinning forces, domain d_1 will also be pinned by a polarization force due to the coupling between the two domains. This force will depend on the phase difference $\phi_1 - \phi_2$ as well as the CDW amplitude Δ_2 at the ultrastrong impurity. This CDW amplitude will also depend on this phase difference $\phi_1 - \phi_2$; Δ_2 will decrease as the phase polarization increases. Lastly, the phase ϕ_2 in the impurity domain d_2 is completely pinned by the ultrastrong impurity situated within it. Hence, ϕ_2 is constant when Δ_2 is nonzero; when Δ_2 drops to zero because of phase polarization, ϕ_2 can hop by a factor of 2π to relieve the phase polarization forces on both domains. A discrete set of hydrodynamical equations which embody these physical mechanisms are given by[15,16]

$$\frac{d\phi_1}{dt} = e - \sin\phi_1 - \alpha\Delta_2(\phi_1 - \phi_2) , \tag{7}$$

$$\phi_2 = \begin{cases} \phi_2, & \Delta_2 > 0 \\ \phi_2 + 2\pi, & \Delta_2 = 0 , \end{cases} \tag{8}$$

$$\Gamma \frac{d\Delta_2}{dt} = 1 - \Delta_2 - \left[\frac{\phi_1 - \phi_2}{\theta} \right]^2 , \tag{9}$$

where e (≥ 0) is the applied electric field, α is the phase mode elasticity coefficient ($\alpha = 2/\varepsilon$ where ε is the Fukuyama-Lee pinning parameter[23]), Γ is the amplitude mode relaxation rate relative to that of the phase mode, and θ is the amplitude mode elasticity coefficient. These equations successfully predict hysteretic CDW switching behavior.[16] In addition, numerical calculations which include the effects of an applied ac field in addition to a dc field indicate that these equations also successfully predict period-doubling routes to chaos, inductive ac response, and mode locking.[15] Thus, the phase-slip model of switching as expressed in Eqs. (7)–(9) provides a simple yet realistic dynamical model of CDW switching. Switching occurs in this model due to the large phase polarization and subsequent amplitude collapse which arises from the extreme phase pinning at an ultrastrong impurity site.

With the fundamental physical principles of switching in mind, we now analyze the experimental results presented in Sec. III in order to determine the way in which the switch-causing ultrastrong impurities are distributed in switching crystals. We also wish to establish the effect this distribution has on the *I-V* characteristics of switching samples.

The thermal gradient effects on the type-I sample depicted in Fig. 2(a) indicates that a temperature difference as small as 2 K is sufficient to break a phase-velocity coherent switching domain into four subdomains over a distance of only 300 μm. This length is far smaller than the sample length required for a thermal gradient to divide this type of domain in a nonswitching sample of $NbSe_3$.[18–22] The much larger effect in type-I switching samples clearly indicates that CDW impurity pinning is nonuniform within type-I switching domains. These apparently coherent switching domains must actually consist of a number of coupled subregions with an average length of not more than 60 μm. These subregions are separated by ultrastrong pinning centers which give rise

to switching behavior. In a nonswitching crystal, the absence of ultrastrong impurities allow large velocity-coherent domains to stay coupled in the presence of relatively large thermal gradients.

The conventional switching behavior of type-II samples is well accounted for by the phase-slip model of switching described by Eqs. (7)–(9).[16] Subdomain coupling and avalanche depinning as observed in type-I switching samples can be accounted for by an extension of this model.[27] We consider a long chain of neighboring domains $d_1 d_2 \cdots d_n$. Each domain is separated from its neighbors by an ultrastrong pinning site US_i which pins the CDW phase in the interface (US_i lies between domains d_i and d_{i+1}). By extending the dynamical phase-slip equations [Eqs. (7)–(9)] we have the following set of differential equations which describe the dynamics of this chain of subdomains:

$$\frac{d\phi_i}{dt} = e - V_i \sin\phi_i - \Delta_{i-1}\alpha_{i-1}(\phi_i - \psi_{i-1}) - \Delta_i \alpha_i (\phi_i - \psi_i) , \tag{10}$$

$$\psi_i = \begin{cases} \psi_i, & \Delta_i > 0 \\ \psi_i + 2\pi, & \Delta_i = 0 , \end{cases} \tag{11}$$

$$\Gamma \frac{d\Delta_i}{dt} = 1 - \Delta_i - \left[\frac{\phi_i - \psi_i}{\theta_i} \right]^2 - \left[\frac{\phi_{i+1} - \psi_i}{\theta_i} \right]^2 , \tag{12}$$

where e (≥ 0) is the applied electric field, V_i is the weak impurity strength in domain d_i, α_i is the phase elasticity coefficient associated with the impurity US_i, Γ is the amplitude relaxation rate relative to that of the phase mode, and θ_i is the amplitude elasticity coefficient at the site US_i; the phase of domain d_i is ϕ_i, while the phase and amplitude of the site US_i are given by ψ_i and Δ_i, respectively. Equation (10) indicates that the phase in domain d_i is pinned by polarization forces stemming from the ultrastrong impurities on either side of it. Similarly, Eq. (12) indicates that the CDW amplitude at an impurity site US_i, Δ_i, is affected by the phase polarization between it and the two weakly pinned domains which it lies between. In the absence of coupling, each subdomain would have an intrinsic switching threshold field E_i; for simplicity we assume that domain d_1 depins first ($E_1 < E_{i\neq 1}$). In the presence of an electric field $E < E_1$ directed from d_1 to d_n, the CDW in each domain becomes polarized in the direction of the field. As indicated by Eq. (10), there will be three pinning forces acting on each domain d_i: $F_i = f_w + f_{i-1} + f_i$, where f_w is due to weak impurities while f_i and f_{i-1} are due to the CDW phase contraction and elongation at the ultrastrong pinning sites in front of and behind the domain, respectively. When E exceeds E_1, Δ_1 will go to zero and domain d_1 depins. The periodic collapse of the CDW at US_1 will periodically eliminate one-half of the phase distortion pinning force acting on d_2 (f_1 will go to zero). This reduction of the pinning force acting on the CDW in domain d_2 may allow it to also depin. If this occurs, the same coupling process can depin domain d_3, then d_4 and so on. Thus, a domain d_i can be triggered to depin when domain d_{i-1} depins if the initial depinning field E_1 is sufficient to overcome the reduced pinning force $F_i = f_w + f_i$. This process of synchronized, triggered depinning is a direct result of the coupling that occurs between neighboring domains when the CDW amplitude collapses at the ultrastrong pinning site which lies between them.

To quantitatively show that the phase-slip model can account for synchronized depinning we have numerically integrated a subset of Eqs. (10)–(12). This subset consists of two weakly pinned domains and two ultrastrong impurity sites arranged serially in the following manner: d_1-US_1-d_2-US_2. The equations which describe the dynamics of this system are

$$\frac{d\phi_1}{dt} = e - V_1 \sin\phi_1 - \Delta_1 \alpha_1 (\phi_1 - \psi_1) , \tag{13}$$

$$\frac{d\phi_2}{dt} = e - V_2 \sin\phi_2 - \Delta_1 \alpha_1 (\phi_2 - \psi_1) - \Delta_2 \alpha_2 (\phi_2 - \psi_2) , \tag{14}$$

$$\psi_1 = \begin{cases} \psi_1, & \Delta_1 > 0 \\ \psi_1 + 2\pi, & \Delta_1 = 0 , \end{cases} \tag{15}$$

$$\Gamma \frac{d\Delta_1}{dt} = 1 - \Delta_1 - \left[\frac{\phi_1 - \psi_1}{\theta_1} \right]^2 - \left[\frac{\phi_2 - \psi_1}{\theta_1} \right]^2 , \tag{16}$$

$$\psi_2 = \begin{cases} \psi_2, & \Delta_2 > 0 \\ \psi_2 + 2\pi, & \Delta_2 = 0 , \end{cases} \tag{17}$$

$$\Gamma \frac{d\Delta_2}{dt} = 1 - \Delta_2 - \left[\frac{\phi_2 - \psi_2}{\theta_2} \right]^2 , \tag{18}$$

where ϕ_1 (ϕ_2) is the phase of domain d_1 (d_2), and ψ_1 (ψ_2) and Δ_1 (Δ_2) are the phase and amplitude of impurity site US_1 (US_2), respectively. For simplicity we assume that the parameters which characterize the weakly pinned domains are exactly the same while the strengths of the two ultrastrong pinning sites are different. This is manifested in the model by the two different amplitude elasticity constants θ_1 and θ_2 (stronger pinning leads to a softer amplitude mode and a smaller elasticity constant). The two weakly pinned domains have the same pinning potentials ($V_1 = V_2$) as well as the same phase elasticity constants ($\alpha_1 = \alpha_2 = 0.2$, corresponding to a Fukuyama and Lee pinning parameter of $\varepsilon = 10$). In addition we assume that both the phase and amplitude modes have the same relaxation rates ($\Gamma = 1$). The calculated I-V characteristics of this CDW system are depicted in Fig. 9 with two sets of amplitude elasticity constants. In Fig. 9(a) the impurity in US_2 is weaker than that in US_1 ($\theta_1 = 10\pi$, $\theta_2 = 15\pi$). The I-V curve clearly shows that this set of parameters leads to two independent, unsynchronized depinnings. The depinning of d_1 is unable to trigger d_2 because the amplitude mode in US_2 is far stiffer than the amplitude mode of US_1. In Fig. 9(b) the impurities in both ultrastrong pinning sites are the same ($\theta_1 = 10\pi$,

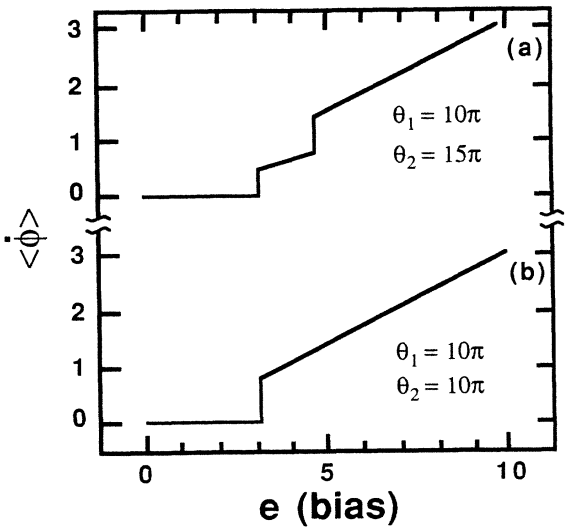

FIG. 9. *I-V* characteristics obtained by integrating the two domain phase-slip equations [Eqs. (13)–(18)] using two different values for the amplitude elasticity coefficient of the second phase-slip center: (a) $\theta_2=15\pi$ and (b) $\theta_2=10\pi$. In both cases the other parameters are $V_1=V_2=1.0$, $\theta_1=10\pi$, $\alpha_1=\alpha_2=0.2$, and $\Gamma=1.0$.

$\theta_2=10\pi$). In this case synchronized depinning does occur. Domain d_2 is able to depin when domain d_1 depins because both ultrastrong pinning sites are of similar strength. In general, domain d_2 is triggered to depin by the depinning of d_1 as long as $\theta_2 \leq \theta_1$. Hence, the phase-slip model of switching can successfully account for both synchronized and unsynchronized subdomain switch depinning.

The triggered depinning process involves a simple linear coupling, and as a result, a chain of synchronized domains will be highly susceptible to the effects of external perturbations. Considering again the chain of n subdomains, if the coupling between domains d_i and d_{i+1} were to break down, all the domains $d_{j>i}$ would no longer take part in synchronized depinning. The fragile nature of the avalanche process indicates why type-I samples are so highly affected by external perturbations. In particular, a thermal gradient destroys the long coupled chain of subdomains which cause large type-I switches because it changes the depinning conditions along the length of the crystal. As a result, a given subdomain may no longer be triggered to depin by its neighbor's depinning. Similarly, type-I switches are highly perturbed when a fine wire is lightly pressed to a sample because the resulting mechanical stress can have a strong effect on the coupling between adjacent subdomains. The data in Fig. 4 suggest that the presence of the perturbing wire in the middle of that crystal destroys the coupling between subdomains near the wire. The sublevels which have been observed in hysteretic type-I switches must also arise from the fragile coupling which exists between subdomains.[4] Sublevels are created when coupling intermittently breaks down between subdomains along a type-I chain of coupled subdomains. This intermittent break may result from subtle temperature or electric field fluctuations.

Type-II $NbSe_3$ and Fe_xNbSe_3 samples show no synchronized depinning effects. In particular, the switches that occur in these materials are unperturbed by either thermal gradients or the mechanical stress brought on by a movable voltage probe. This indicates that there is actually no coupling between neighboring domains in these materials. Hence, neighboring domains are completely independent and depin according to their local conditions. It is important to note that the CDW pinning strengths of the impurities which cause switching in type-II $NbSe_3$ are similar to those found in type-I samples. This is evident from the fact that the switching threshold fields are roughly the same in these two classes of switching $NbSe_3$. Thus, the lack of domain coupling in type-II samples cannot be attributed to stronger pinning in those crystals.

A typical type-II switching domain is much larger than the small subdomains which give rise to switching in type-I $NbSe_3$. This is evident in the results presented in the previous section; in samples of roughly equal length, a type-I $NbSe_3$ crystal was composed of ten switching domains while the type-II sample consisted of four domains. This indicates that the separation between the ultrastrong impurities has a direct bearing on whether or not neighboring domains can couple together when depinning. To clarify the situation, we define a length scale L_{us} which is the average distance between neighboring ultrastrong impurities; in addition, L_c is defined as the critical separation beyond which adjacent domains do not interact. Within this framework type-I samples are characterized by $L_{us}<L_c$. In this case coupling does occur between adjacent domains and this causes synchronized depinning and the many effects associated with it (i.e., large switches, sublevels, ΔT switch breakup). Both type-II samples of $NbSe_3$ and all samples of Fe_xNbSe_3 correspond to $L_{us}>L_c$. In this case there can be no switch domain coupling. As a result, the switches in these samples are unaffected by external perturbations.

There are two possible explanations for why the coupling mechanism can break down when $L_{us}>L_c$. First, it may be that when created in the crystal-growth process, closely spaced impurities have equivalent pinning strengths, while the strengths of widely separated impurities differ considerably. It is also possible that the coupling effects on a domain decrease as the domain becomes larger; the reduction in the pinning force on a large domain due to the periodic collapse of the CDW at the interface with a depinned neighbor might not be a large enough effect to allow synchronized depinning. A combination of these two effects is probably influential in undermining the coupling mechanism between large type-II domains. Regardless of the underlying mechanisms, the behavior of many type-I and type-II $NbSe_3$ samples indicates that the critical ultrastrong impurity separation is roughly $L_c \simeq 200\ \mu m$.

V. CONCLUSION

The widely varying *I-V* characteristics observed in $NbSe_3$ switching samples can be accounted for by differences in the distribution of the ultrastrong impuri-

ties which cause switching. When the impurities are closely spaced, coupling can occur between adjacent switching domains. This allows a depinning wave to move along the length of the crystal, creating a large switch in the *I-V* curve. The mechanism which links neighboring domains is fragile and is easily destroyed by the application of external perturbations. Conversely, widely spaced impurities do not allow adjacent domains to interact. With no interdomain coupling, these materials depin via a number of small switches which are unaffected by external perturbations. Hence, we propose that the drastically different behavior observed in type-I and type-II switching samples is simply a manifestation of the different distributions of ultrastrong impurities contained within them.

Iron-doped $NbSe_3$ displays only small switches which are unaffected by external perturbations. These samples show no synchronized depinning behavior. This indicates that the impurities in Fe_xNbSe_3 are widely spaced. No coupling occurs between adjacent domains and each switching domain behaves independently of the other domains.

These results have important implications for the physical arrangement of the impurities which cause switching. In the case of iron-doped $NbSe_3$, these impurities are not plentiful. This suggests that the iron dopant is not uniformly distributed throughout a crystal. With regard to pure $NbSe_3$, the ultrastrong impurities can be quite plentiful, giving rise to type-I behavior, or extremely sparse, resulting in type-II behavior. The closest separation between adjacent impurities inferred from thermal gradient experiments is $L_{us} \approx 40$ μm which is roughly in line with the density of grain boundaries and twinning defects observed in $NbSe_3$.[28] Further research employing TEM and advanced microprobe analysis is needed to determine the precise nature of the impurities which cause switching in $NbSe_3$.

ACKNOWLEDGMENTS

We thank P. Parilla and M. Sherwin for useful discussions. This research was supported by National Science Foundation (NSF) Grant No. DMR-84-00041. One of us (A.Z.) acknowledges support from the Alfred P. Sloan Foundation.

[1]For a review, see G. Grüner and A. Zettl, Phys. Rep. **119**, 117 (1985).
[2]A. Zettl and G. Grüner, Phys. Rev. B **26**, 2298 (1982).
[3]R. P. Hall and A. Zettl, Solid State Commun. **50**, 813 (1984).
[4]R. P. Hall and A. Zettl, Solid State Commun. **57**, 27 (1986).
[5]R. P. Hall, M. Sherwin, and A. Zettl, Phys. Rev. Lett. **52**, 2293 (1984).
[6]R. P. Hall, M. Sherwin, and A. Zettl, Phys. Rev. B **29**, 7076 (1984).
[7]R. P. Hall and A. Zettl, Solid State Commun. **55**, 307 (1985).
[8]L. Mihaly and G. Grüner, Solid State Commun. **50**, 807 (1984).
[9]J. Dumas, C. Schlenker, J. Marcus, and R. Buder, Phys. Rev. Lett. **50**, 757 (1983).
[10]Z. Z. Wang, P. Monceau, M. Renard, P. Gressier, L. Guemas, and A. Meerschaut, Solid State Commun. **47**, 439 (1983).
[11]M. P. Everson and R. V. Coleman, Phys. Rev. B **28**, 6659 (1983).
[12]H. Mutka, S. Bouffard, J. Dumas, and C. Schlenker, J. Phys. (Paris) Lett. **45**, L729 (1985).
[13]R. P. Hall, M. F. Hundley, and A. Zettl, Phys. Rev. Lett. **56**, 2399 (1986).
[14]R. P. Hall, M. F. Hundley, and A. Zettl (unpublished).
[15]M. Inui, R. P. Hall, S. Doniach, and A. Zettl (unpublished).
[16]R. P. Hall, M. F. Hundley, and A. Zettl, Physica B + C **143B**, 152 (1986).
[17]M. F. Hundley and A. Zettl, Solid State Commun. **65**, 791 (1988).
[18]X. J. Zhang and N. P. Ong, Phys. Rev. B **30**, 7343 (1984).
[19]A. Zettl, M. Kaiser, and G. Grüner, Solid State Commun. **53**, 649 (1985).
[20]S. E. Brown, A. Janossy, and G. Grüner, Phys. Rev. B **31**, 6869 (1985).
[21]M. F. Hundley and A. Zettl, Phys. Rev. B **33**, 2883 (1986).
[22]J. W. Lyding, J. S. Hubacek, G. Gammie, and R. F. Thorne, Phys. Rev. B **33**, 4341 (1986).
[23]H. Fukuyama and P. A. Lee, Phys. Rev. B **17**, 535 (1978).
[24]N. P. Ong, G. Verma, and K. Maki, Phys. Rev. Lett. **52**, 663 (1984).
[25]N. P. Ong and K. Maki, Phys. Rev. B **32**, 6582 (1985).
[26]Other models of switching have been proposed. See B. Joos and D. Murray, Phys. Rev. B **29**, 1094 (1984); W. Wonneberger and H. J. Breymayer, Z. Phys. B **56**, 241 (1984); also A. Janossy, G. Mihaly, and L. Mihaly, in *Charge Density Waves in Solids*, edited by Gy. Hutiray and J. Solyom (Springer, New York, 1985), p. 412; and L. Mihaly, Ting Chen, and G. Grüner, Solid State Commun. **61**, 751 (1987).
[27]It is interesting to note that the concept of domain coupling and avalanche depinning is similar to a model first proposed in B. Joos and D. Murray, Phys. Rev. B **29**, 1094 (1984).
[28]J. L. Hodeau, M. Marezio, C. Roucau, R. Ayroles, A. Meerschaut, J. Rouxel, and P. Monceau, J. Phys. C **11**, 4117 (1978).